Renewable Energy, Environment, and Power Quality Journal (REE&PQJ)
ISSN:3020-531X
Volume 26, July 2026

High-Capacity Conductor Data-Based Models for Dynamic Rating of Electrical Lines

Julio J. Melero, M.Paz Comech. and José F. Sanz

InstitutoUniversitario de Investigación Mixto de la Energía y la Eficiencia de los Recursos de Aragón, ENERGAIA
Universidad de Zaragoza-Fundación CIRCE
Mariano Esquillor 15, 50018 Zaragoza, Spain. +34976762402, melero@unizar.es

Abstract. Accurate estimation of overhead conductor temperature is a key requirement for reliable dynamic line rating (DLR) and enhanced utilization of transmission networks. This paper presents a data-driven framework based on XGBoost regression to predict conductor temperature from electrical loading and meteorological variables. Hyperparameters are optimized using an Optuna-based search with controlled model complexity to ensure robust generalization. Model interpretability is addressed through SHAP analysis, which confirms that the learned relationships are physically consistent with established IEEE 738 and CIGRÉ thermal principles. To quantify predictive uncertainty, conformal prediction is integrated, providing statistically valid temperature intervals that support risk-aware ampacity assessment. The proposed approach achieves high predictive accuracy on real-world data while delivering transparent and reliable uncertainty estimates. Results demonstrate that the framework is a practical and scalable solution for DLR applications, enabling increased line utilization without compromising thermal safety margins.

Keywords. Overhead transmission lines, ampacity, conductor temperature, weather parameters, machine learning.

1. Introduction

The current deployment of renewable energy sources, together with rising energy demand, is creating serious problems for electricity distribution and transmission companies. The energy transition to a decarbonized electricity system involves installing more and more renewable generation plants, which are causing congestion and bottlenecks in the current power transmission and distribution networks. This also means possible production limitations for generation systems to maintain safe and reliable operating conditions on existing lines.

The aforementioned problems could be solved by developing new lines, the technically simplest option. However, administrative, environmental, and, of course, economic issues prevent new developments. Therefore, the focus has been on increasing the capacity of existing lines. Among the available options [1-5], increasing the ampacity, or maximum current that the line can carry, has been the most studied in recent years. Line capacity and conductor temperature can be estimated from meteorological measurements and the current flowing through the line, enabling dynamic rating management (DRM) [2]. Recent advances in this technique allow system operators to manage networks in real time, leveraging higher transmission capacities based on actual weather conditions.

DRM strategies use two key parameters: conductor temperature (Tc) and maximum permissible current, or ampacity (Imax). In temperature-based DRM, the conductor temperature is estimated in real time, enabling operators to increase or decrease the line current safely. On the other hand, ampacity-based DRM determines the optimal line load capacity subject to conductor thermal constraints [6-7]. When combined with other flexibility options, these approaches significantly improve the power grid's operational capacity and adaptability [8,9].

The use of last-generation conductors that allow higher currents to flow while maintaining excellent thermal and mechanical properties is currently becoming more widespread. This is the case with High-Temperature, Low-Sag (HTLS) conductors, which can withstand higher temperatures and whose current-carrying capacity increases as the maximum operating temperature rises. However, existing theoretical models have not been extensively tested on these conductors, which can carry current densities much higher than conventional conductors.

The theoretical calculation models currently in use are based on the analysis of thermal equilibrium under typical operating conditions for conventional conductors. The IEEE 738 [6] and CIGRÉ [7] models show good performance in estimating the operating conditions of conventional conductors with low current densities and operating temperatures below 100 °C, yielding similar results [8]. Beyond the results obtained under controlled conditions, it is clear that multiple factors influence the models, and their performance shows discrepancies in real-world situations, where they do not provide accurate results even at low current densities [9]. Furthermore, the application of these methodologies under high-load and high-temperature conditions, as is the case with HTLS conductors, can lead to greater discrepancies between the two models and actual conditions [10-12].

This work proposes a new data-driven approach to accurately estimate the temperature of an HTLS conductor. To this end, we used data from a pilot facility with an HTLS conductor and applied two regression models: linear regression and gradient boosting. The following sections describe the materials, data, and methods used; the results obtained; the discussion of the relationship between the numerical model results and the problem's physics; and the conclusions drawn.

2. Materials and Methods

A. Description of the facility

The prototype consists of an HTLS conductor, specifically the "Nexans ACSS/TW/AW 133/22," connected in a current loop of up to 1600 A and installed outdoors to subject it to real operating conditions.

Two PT100 probes were placed on the conductor to measure its temperature, as shown in Fig. 1, which presents a general view of the setup. A weather station was installed next to the current loop to record the ambient temperature. Two PT100 probes, T1 and T2, were placed on the conductor to measure its temperature (see Fig. 1). A datalogger was installed next to the current loop to record the ambient temperature, wind speed, wind direction, solar radiation, and relative humidity. In addition, the two PT100 probes used to measure the conductor temperature were connected to the datalogger to synchronize them with the other measured variables. A complete description of the system can be found in [10].

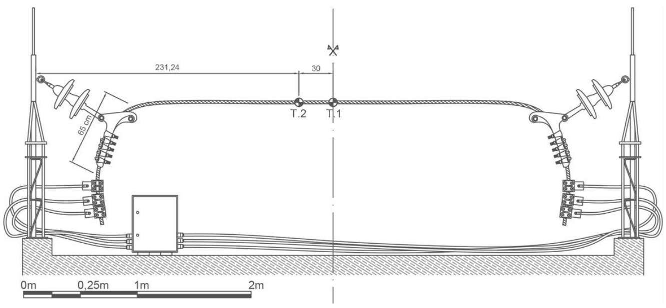

Fig. 1. General view of the experimental setup [10].

B. Data collection, cleaning, and feature engineering

Data were recorded at 1/60 Hz, i.e., one register per minute from 12/12/2023 to 3/19/2024 [13]. The original dataset contained 327669 records with 11 columns. The columns contained the date, conductor temperature 1 (T1), conductor temperature 2 (T2), solar radiation, conductor current, ambient temperature, relative humidity, wind speed, wind direction, conductor orientation angle, and wind angle (obtained by subtracting the conductor orientation angle from the wind direction).

Downloaded data were thoroughly reviewed, with null or incorrect values discarded as likely due to measurement errors. In the cleaned dataset, unnecessary columns were dropped, and certain transformations were applied to fit regression models and estimate the conductor temperature from the other relevant variables. First, the date and time column was discarded because the regression would not be performed on a time series. Next, as the wind direction and conductor orientation columns contained duplicate information that was already reflected in the wind angle attack, they were also discarded. Finally, since the variable to be estimated was the conductor temperature, the two columns, T1 and T2, were combined into a single column, with a new column, called *position*, indicating the position at which each temperature was measured. To do this, the data were duplicated, keeping T1 in the first half and assigning 1 to the position value, while T2 was kept in the second half and assigned the value 2 to the position. This feature engineering was derived from the temperature profiles observed on the prototype [10].

The final dataset contained 344410 records, which were randomly split into *training*, *cal,* and *test* sets in a 70/15/15 proportion, with 241086 records in the training set and 51662 in the *cal* and *test* sets. Randomizing the split is important because it maintains the same data distribution across all sets and avoids feature autocorrelation. The data distributions were verified to ensure consistency across the three splits.

C. Methodology

To provide a simple reference, a multivariate linear regression model was selected first. This parametric model allows for clear visualization of linear dependencies (if any) between conductor temperature and explanatory variables. It also serves as a reference for quantifying the added value of more advanced models.

Given that the problem is clearly nonlinear, a gradient boosting method [14] was selected for its ability to accurately model complex nonlinear relationships and feature interactions without explicitly specifying the underlying functional form. This method combines the predictions of a group of 'weak' learners, integrating them into a strong learner through cumulative training steps. The cumulative learning process is as follows. First, the initial learner is fitted to the entire input data space. Next, the second model is trained with the residuals of the first learner. To improve the 'weak' learners' capabilities, the process is repeated until a stopping condition is satisfied. The final result is calculated by adding the predictions of all learners.

XGBoost [15] was selected among gradient boosting algorithms for its high predictive accuracy, computational efficiency, and robustness when applied to large-scale tabular datasets. It features advanced regularization capabilities that enable stable training and strong generalization across various operating conditions. Furthermore, its compatibility with GPU acceleration and model interpretability tools makes XGBoost particularly well-suited for the problem under study.

Regression performance is assessed using the root mean square error (RMSE), the mean absolute error (MAE), and

the coefficient of determination (R^2). RMSE and MAE quantify the prediction error magnitude, while R^2 measures the proportion of variance in the target variable explained by the model.
Once the point prediction has been obtained using the gradient boosting algorithm, it is essential to explicitly quantify the uncertainty associated with that estimate. In operationally critical applications, such as DLR, point predictions alone are insufficient to ensure safe decision-making in variable environmental conditions. For this reason, conformal prediction [16, 17] was used to construct uncertainty intervals, given its distribution-free and model-agnostic formulation, which guarantees valid coverage levels (e.g., 85%, 90%, and 99%) with minimal assumptions. Using a dedicated calibration dataset (*cal* set) in this study, conformal prediction provides data-adaptive uncertainty bounds for conductor temperature**,** enabling risk-aware ampacity assessment without compromising predictive accuracy.

Finally, to interpret the influence of the different features on the predicted conductor temperature, SHAP (Shapley Additive exPlanations) [18] values were employed. SHAP provides an additive decomposition of the model's output by assigning a marginal contribution to each feature using cooperative game theory, enabling both global and local interpretability. This approach allows the identification of dominant drivers, nonlinear effects, and operating regimes, thereby facilitating a physically meaningful interpretation of the data-driven model.

D. Hardware and Software Environment

The computational platform used in this work is based on a 12th Gen Intel® Core™ i9-12900K processor with a hybrid architecture comprising 32 logical cores, complemented by 128 GB of system RAM. For hardware acceleration, the system is equipped with two NVIDIA GeForce RTX 3090 GPUs, providing high computational performance for data-intensive workloads.

The software environment is based on Python and leverages GPU acceleration through CUDA. Gradient boosting models are implemented using XGBoost, with hyperparameter optimization performed via Optuna [19]. Uncertainty quantification is addressed through conformal prediction to provide statistically valid prediction intervals. At the same time, SHAP supports model interpretability, enabling a transparent analysis of feature contributions to the predicted conductor temperature.

3. Results

A. Multivariate linear regression

The linear regression model exhibits limited predictive capability, as reflected in the metrics shown in Table I for the *test set*.

Table I. – Multivariate linear regression metrics

RMSE	MAE	R^2
17.62 ºC	12.81 ºC	0.77

The relatively high error metrics indicate a poor agreement between predicted and observed values. At the same time, the low R^2 suggests that the linear model cannot capture a significant portion of the variability in the target variable. These results highlight the limitations of linear assumptions for this regression problem and motivate the use of more flexible nonlinear models.

B. XGBoost training

XGBoost hyperparameters were tuned using Optuna via Bayesian optimization, with candidate configurations evaluated by minimizing RMSE on an independent validation set and early stopping. This automated procedure enables an efficient search of the hyperparameter space while controlling model complexity. The optimization run for 3000 trials over approximately 4 hours, using both GPUs in parallel.

Table II. – Final XGBoost hyperparameters

Hyperparameter	Value
n_estimators	1500
max_depth	9
learning_rate	0.20
subsample	0.83
colsample_bytree	0.89
min_childweigth	8
gamma	0.30
reg_alpha	0.94
reg_lambda	1.01

The boosting procedure was allowed to run for up to 1500 trees. As a result, the final model retained the complete set of 1500 boosting trees, achieving a stable balance between predictive accuracy and model complexity without unnecessary overfitting. The final set of hyperparameters is shown in Table II for reproducibility. These values were used to train the final XGBoost model for conductor temperature estimation.

Table III. – XGBoost regression metrics

	RMSE	MAE	R^2
cal-set	3.52 ºC	1,98 ºC	0.991
test-set	3.56 ºC	2.00 ºC	0.991

B. Final model

The hyperparameters shown in Table II were used to fit the definitive model on the training dataset. Table III shows the model metrics calculated on the independent *cal* and *test* datasets. The ideal fit (y = x) is also shown to highlight the model's goodness-of-fit.

Fig. 2 compares the predicted and measured conductor temperatures, providing a visual assessment of the model's performance and confirming strong agreement between the estimated and observed values across the operating range.
The model results were better than those obtained with the classical thermal models [6-7], as shown in a previous paper using these data [10].

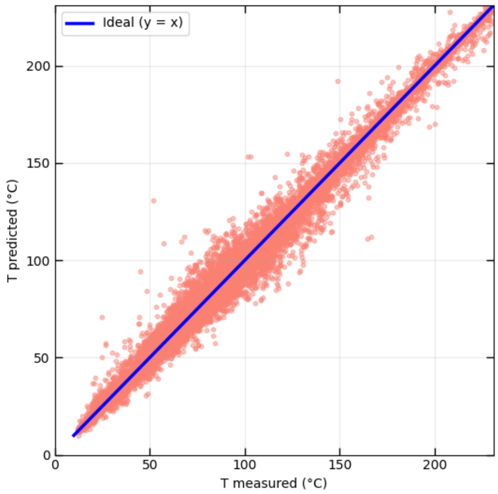

Fig. 2. Predicted vs measured conductor temperature.

C. Confidence intervals

The conformal prediction intervals were calibrated on the *cal* dataset using the residuals from the conductor temperature model. The resulting mean widths were ±4.58°C, ±7.12°C, and ±14.88°C for nominal coverage levels of 90%, 95%, and 99%, respectively, reflecting the increasing uncertainty required to ensure greater reliability. When evaluated on the independent test set, the empirical coverages closely matched the nominal values, reaching 89.8%, 94.9%, and 99.0%, respectively. This close agreement confirms the validity and robustness of the conformal calibration, demonstrating that the proposed uncertainty limits generalize well beyond the calibration data. These results indicate that conformal prediction provides reliable, data-driven uncertainty quantification for conductor temperature estimation, supporting risk-aware decision-making in dynamic line classification applications.

Fig. 3 displays a sample from the test dataset, including the measured and predicted data, along with the 90%, 95%, and 99% calculated confidence intervals. X-axis labels are not shown because the data were disordered and lacked meaning.

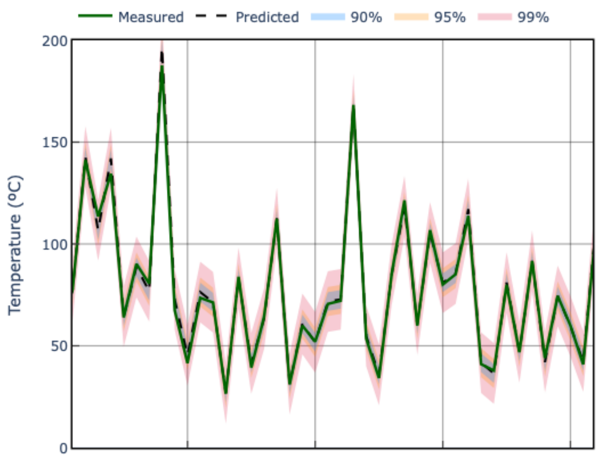

Fig. 3. Sample of predicted and measured conductor temperature on the *test* set, including conformal prediction intervals at 90%, 95%, and 99% coverage levels.

D. Feature importance

The adjusted XGBoost model functions as a black box, and it is necessary to delve deeper into the importance and influence of the variables used in the final result. For this purpose, the SHAP methodology was used.
Fig. 4 summarizes the global importance of the input variables in the XGBoost model through mean absolute SHAP values, revealing the relative contribution of each feature to the predicted conductor temperature. Line current clearly dominates, confirming Joule heating as the primary driver of thermal behavior and ampacity constraints, in agreement with thermal balance formulations. Wind speed and ambient air temperature follow in importance, highlighting the key role of convective cooling and ambient thermal conditions. Wind angle also exhibits a relevant contribution, underscoring the influence of wind–conductor orientation on cooling efficiency. In contrast, relative humidity, solar radiation, and sensor position show a comparatively minor impact, indicating a secondary role under the analyzed conditions. Overall, the SHAP-based analysis confirms that the model captures the main physical mechanisms governing conductor temperature.

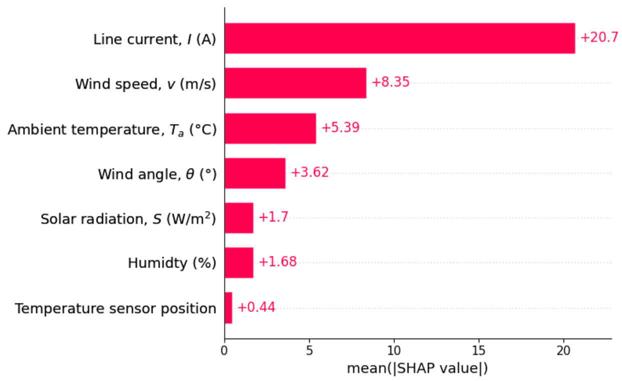

Fig. 4. Global feature importance based on mean absolute SHAP values.

D. Discussion

Fig. 5 provides a detailed SHAP dependence analysis of the XGBoost regression model used to predict conductor temperature, allowing both the magnitude and the functional form of each variable's influence to be examined. Each panel (a–f) shows the SHAP marginal contribution as a function of the corresponding input variable, together with binned quantile trends and automatically detected regime-change points.

Panel (a) confirms that line current is the dominant driver of conductor temperature, exhibiting a strongly nonlinear relationship. At lower current levels, the marginal contribution increases moderately, whereas beyond a critical threshold, the SHAP values rise sharply, indicating a regime in which Joule losses dominate the thermal balance. This transition is consistent with the quadratic dependence of resistive heating on current and explains the high regime-change strength identified for this variable.

Panel (b) illustrates the effect of solar radiation, which shows a comparatively weaker and slightly decreasing marginal contribution. This behavior suggests that, under the analyzed operating conditions, solar heat gains play a secondary role, although their contribution remains consistently positive.

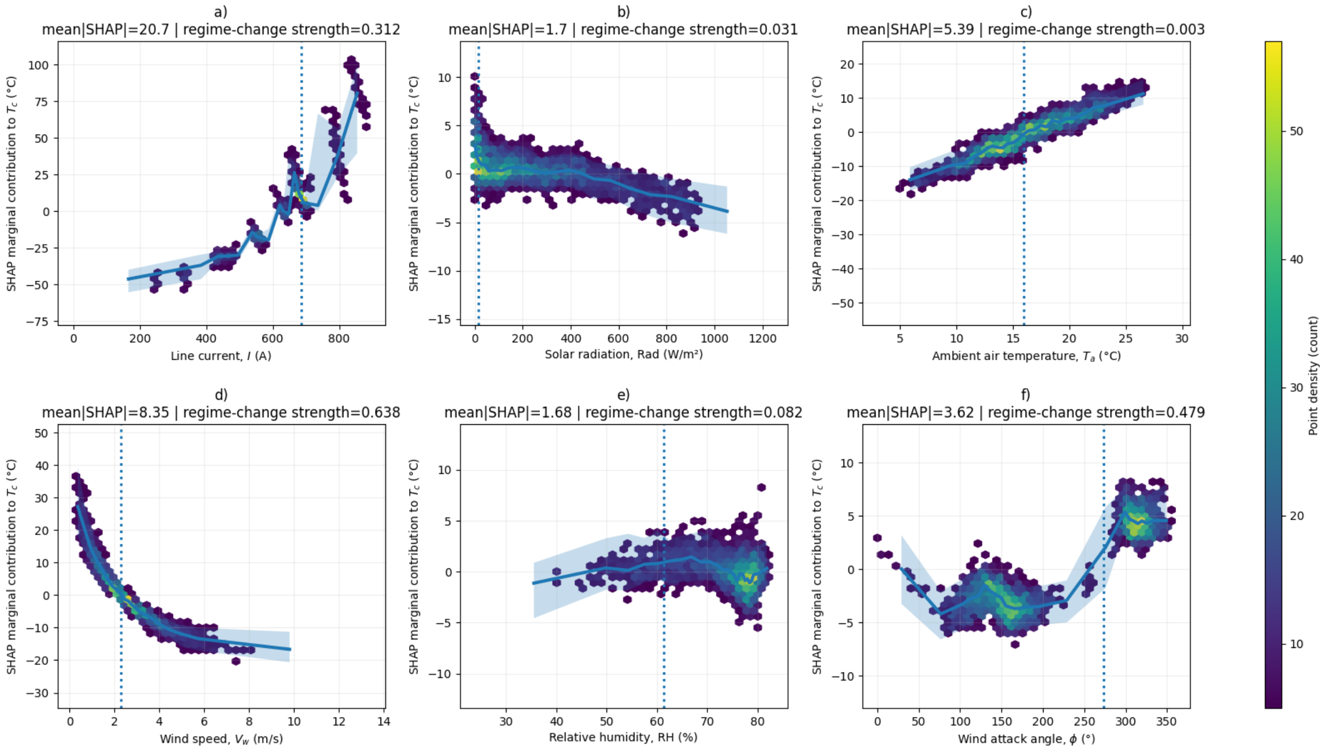

Fig. 5. SHAP dependence plots for the XGBoost conductor temperature model, illustrating the marginal contribution of each input variable and highlighting regime-change points that reveal nonlinear thermal behavior relevant to dynamic line rating.

Panel (c) highlights a nearly linear and monotonic relationship between ambient air temperature and conductor temperature contribution. Higher ambient temperatures reduce the thermal gradient between the conductor and the surrounding air, leading to systematically higher conductor temperatures, as reflected by the steadily increasing SHAP values.

Panel (d) demonstrates the strong cooling effect of wind speed, with SHAP contributions decreasing sharply as wind velocity increases. The curve flattens at higher wind speeds, indicating diminishing marginal cooling benefits once forced convection becomes dominant. The pronounced regime change observed in this panel reflects the transition between low- and high-wind cooling regimes, as described in IEEE 738 [6] and CIGRÉ [7].

Panel (e) shows that relative humidity has a limited influence on conductor temperature, with SHAP values clustered near zero and no clear regime transition. This confirms that humidity effects are primarily indirect and of minor importance compared to other meteorological variables in the studied dataset.

Finally, panel (f) reveals a highly nonlinear dependence on the wind attack angle, with apparent regime shifts. Minimum cooling effectiveness is observed for oblique wind directions. At the same time, near-perpendicular angles lead to a marked increase in convective cooling efficiency, as reflected by the sharp change in SHAP contributions. This result underscores the importance of explicitly accounting for wind–conductor orientation in dynamic line rating applications.

Overall, it has been demonstrated that the proposed XGBoost model captures not only the relative importance of the input variables but also the physically meaningful nonlinear regimes governing the thermal behavior of the conductor. The consistency between the SHAP-based interpretation and established thermal principles reinforces the model's suitability for reliable, interpretable dynamic ampacity assessment.

4. Conclusion

This study demonstrates that a data-driven approach based on XGBoost can accurately and reliably predict overhead conductor temperature, achieving high predictive performance while preserving physical interpretability. The model successfully captures the dominant thermal mechanisms governing conductor behavior, with line current, wind speed, ambient temperature, and wind angle identified as the primary drivers, in agreement with established IEEE 738 and CIGRÉ formulations. The combination of Optuna-based hyperparameter optimization and controlled model complexity selection ensured robust generalization and avoided overfitting. In addition, integrating conformal prediction provides statistically valid uncertainty intervals, enabling risk-aware ampacity assessment and supporting operational decision-making under uncertainty. Once the model has been developed, the computational effort required for real-time deployment is minimal, and inference time is negligible.

Despite these strengths, the proposed methodology presents some limitations. The model performance is inherently dependent on the representativeness and quality of the available measurements, and its generalization to different conductor types, spans, or climatic regimes may require retraining or domain adaptation. Furthermore, transient thermal effects and spatial variability along the line are not explicitly modeled and could influence local temperature dynamics under rapidly changing conditions. Future work will focus on extending the framework to multi-span and multi-conductor scenarios, incorporating additional physical constraints or hybrid physics-informed formulations, and validating the approach under a broader range of operating conditions. The integration of real-time data streams and adaptive uncertainty quantification is also envisaged to further enhance the method's applicability for operational dynamic line rating.

Acknowledgement

The authors wish to thank Luis Vejo and Mario Mañana from the University of Cantabria for sharing the data used in this study.

References

[1] E. Fernandez, I. Albizu, A. J. Mazon, A. Etxegarai, G. Buigues, and R. Alberdi, "Power line monitoring for the analysis of overhead line rating forecasting methods," in *2016 IEEE PES PowerAfrica*, 2016, pp. 119–123. doi: 10.1109/PowerAfrica.2016.7556583.

[2] R. Martinez *et al.*, "Dynamic rating management of overhead transmission lines operating under multiple weather conditions," *Energies (Basel)*, vol. 14, no. 4, Feb. 2021, doi: 10.3390/en14041136.

[3] F. Ye and J. Teh, "Dynamic thermal rating in power systems: A comprehensive review of techniques, implementation and reliability," *Renewable and Sustainable Energy Reviews*, vol. 226, p. 116392, Jan. 2026, doi: 10.1016/j.rser.2025.116392.

[4] X. Zhou, S. Wang, T. Li, J. Cao, Y. Zou, and X. Xiang, "Probabilistic Ampacity Rating of 500kV Overhead Transmission Lines in Zhejiang Province," in *2018 IEEE 3rd International Conference on Integrated Circuits and Microsystems (ICICM)*, 2018, pp. 98–103. doi: 10.1109/ICAM 2018.8596438.

[5] C. Holyk, H. D. Liess, S. Grondel, H. Kanbach, and F. Loos, "Simulation and measurement of the steady-state temperature in multi-core cables," *Electric Power Systems Research*, vol. 116, pp. 54–66, Nov. 2014, doi: 10.1016/J.EPSR.2014.05.001.

[6] IEEE Std 738-2012; IEEE Standard for Calculating the Current-Temperature Relationship of Bare Overhead Conductors. IEEE.Power and Energy Society: Piscataway, NJ, USA, 2013; pp. 1–72; Revision of IEEE Std 738-2006/IEEE Std 738-2012/Cor 1-2013.

[7] Dale, D.; Vincent, M.; Rob, S.; Mark, B.; Dzevad, M.; Ralf, P.; Daniel, G.; Sidnei, U.; Kresimir, B.; Sven, H.; et al. CIGRÉ 601; Guide For Thermal Rating Calculations of Overhead Lines; CIGRÉ: Paris, France, 2014.

[8] A. Arroyo *et al.*, "Comparison between IEEE and CIGRÉ thermal behaviour standards and measured temperature on a 132-kV overhead power line," *Energies (Basel)*, vol. 8, no. 12, pp. 13660–13671, 2015, doi: 10.3390/en81212391.

[9] N. Viafora, K. Morozovska, S. H. H. Kazmi, T. Laneryd, P. Hilber, and J. Holbøll, "Day-ahead dispatch optimization with dynamic thermal rating of transformers and overhead lines," *Electric Power Systems Research*, vol. 171, pp. 194–208, Jun. 2019, doi: 10.1016/j.epsr.2019.02.026.

[10] L. Vejo *et al.*, "Experimental Study of Dynamic Line Rating Applied to High-Temperature Low-Sag Conductors," *Energies (Basel)*, vol. 18, no. 4, Feb. 2025, doi: 10.3390/en18040929.

[11] M. Jalilian, J. R. Riba, and P. Parvizi, "Aluminum Conductor Steel-Supported Conductors for the Sustainable Growth of Power Line Capacity: A Review and Discussion," Sep. 01, 2024, *Multidisciplinary Digital Publishing Institute (MDPI)*. doi: 10.3390/ma17184536.

[12] J. R. Riba, "The Role of AC Resistance of Bare Stranded Conductors for Developing Dynamic Line Rating Approaches," *Applied Sciences (Switzerland)*, vol. 14, no. 19, Oct. 2024, doi: 10.3390/app14198982.

[13] L. Vejo, "Current and temperature measurements for a HTLS Conductor based in Santander ," Dec. 2024, *Zenodo*. doi: 10.5281/zenodo.14274381.

[14] T. ; T. R. ; F. J. H. Hastie, "Boosting and additive trees," in *The Elements of Statistical Learning*, 2nd ed., New York: Springer, 2009, pp. 337–384.

[15] T. Chen and C. Guestrin, "XGBoost: A scalable tree boosting system," in *Proceedings of the ACM SIGKDD International Conference on Knowledge Discovery and Data Mining*, Association for Computing Machinery, Aug. 2016, pp. 785–794. doi: 10.1145/2939672.2939785.

[16] A. Gammerman, V. Vovk, and V. Vapnik, "Learning by transduction," in *Proceedings of the Fourteenth Conference on Uncertainty in Artificial Intelligence*, in UAI'98. San Francisco, CA, USA: Morgan Kaufmann Publishers Inc., 1998, pp. 148–155.

[17] A. N. Angelopoulos and S. Bates, "A Gentle Introduction to Conformal Prediction and Distribution-Free Uncertainty Quantification," Dec. 2022, [Online]. Available: http://arxiv.org/abs/2107.07511

[18] S. M. Lundberg and S.-I. Lee, "A unified approach to interpreting model predictions," in *Proceedings of the 31st International Conference on Neural Information Processing Systems*, in NIPS'17. Red Hook, NY, USA: Curran Associates Inc., 2017, pp. 4768–4777.

[19] T. Akiba, S. Sano, T. Yanase, T. Ohta, and M. Koyama, "Optuna: A Next-generation Hyperparameter Optimization Framework," in *Proceedings of the ACM SIGKDD International Conference on Knowledge Discovery and Data Mining*, Association for Computing Machinery, Jul. 2019, pp. 2623–2631. doi: 10.1145/3292500.3330701.